Magma storage beneath Grímsvötn volcano, Iceland, constrained by clinopyroxene-melt thermobarometry and volatiles in melt inclusions and groundmass glass

B. Haddadi, O. Sigmarsson, G. Larsen

AGU PUBLICATIONS

JGR

Journal of Geophysical Research: Solid Earth

RESEARCH ARTICLE
10.1002/2017JB014067

Key Points:
- Clinopyroxene crystallization of Grímsvötn basalt indicates mid-to-lower crustal magma storage above the Iceland mantle plume
- Different eruption regimes are due to variable recharge of deeper-seated and gas-rich magma recharge
- Sulfur concentration of matrix glass and exsolution budget correlate with known magma volumes

Supporting Information:
- Supporting Information S1
- Table S1
- Table S2
- Table S3

Correspondence to:
O. Sigmarsson,
olgeir@hi.is

Citation:
Haddadi, B., O. Sigmarsson, and G. Larsen (2017), Magma storage beneath Grímsvötn volcano, Iceland, constrained by clinopyroxene-melt thermobarometry and volatiles in melt inclusions and groundmass glass, *J. Geophys. Res. Solid Earth*, *122*, 6984–6997, doi:10.1002/2017JB014067.

Received 3 FEB 2017
Accepted 25 JUL 2017
Accepted article online 4 AUG 2017
Published online 9 SEP 2017

Magma storage beneath Grímsvötn volcano, Iceland, constrained by clinopyroxene-melt thermobarometry and volatiles in melt inclusions and groundmass glass

B. Haddadi[1], O. Sigmarsson[1,2], and G. Larsen[2]

[1]Laboratoire Magmas et Volcans, CNRS - Université Clermont Auvergne - IRD, Campus Universitaire des Cézeaux, Aubière, France, [2]Institute of Earth Sciences, University of Iceland, Reykjavik, Iceland

Abstract Basalt eruptions at Grímsvötn volcano, Iceland, are generally of low intensity; however, occasionally, an order of magnitude larger eruptions occur. In order to discuss the reasons for this difference, the degassing budget of S and Cl and crystallization conditions of the eruptive magma were determined from volatile concentration measured in melt inclusion (MI) and groundmass glass and thermobarometry, respectively. Tephra of two of the largest historical eruptions (2011 and 1873) and two much smaller eruptions (2004 and 1823) were investigated. Sulfur and Cl concentrations are higher in groundmass glass of the smaller eruptions due to incomplete outgassing caused by melt quenching in contact with glacial water. Sulfur concentration and degassing budget correlate with erupted magma volumes. Higher volatile concentrations of MI from the larger eruptions reflect important recharge of gas-rich magma from depth. The recharge causes a high-magnitude eruption followed by increased eruption frequency over the following decades. Pressure and temperature estimates of crystallization are obtained through equilibrium clinopyroxene-glass pairs, where crystals adjacent to, and in textural equilibrium with, both groundmass glass and that of MI were measured. An average crystallization pressure of 4 ± 1 kbar corresponding to approximately 15 ± 5 km depth was obtained together with a considerable temperature range, 1065–1175°C. Similar crystallization depths are obtained for the basalt of the 2014–2015 Bárðarbunga rifting event and to a low resistivity layer revealed by magnetotelluric surveys. Therefore, an important magma storage depth is inferred at lower crustal depth above the center of the Iceland mantle plume.

1. Introduction

Knowing the depth at which magma is stored beneath active volcanoes is important for eruption mitigation and corresponding hazard assessment. The configuration of magma plumbing systems beneath active basaltic volcanoes is principally inferred from geophysical observations. The most densely equipped volcanoes, such as Kīlauea (Hawaii), Etna (Italy), and Piton de la Fournaise (Réunion Island), appear to be characterized by a plexus of dikes and sills or "vertically stacked magma reservoirs" [*Poland et al.*, 2014, and references therein]. At Kīlauea, basalt of different nature allows identifying the relative depth of magma storage, with evolved composition reflecting stagnant or residual magma stored at high-level and more mafic basalt deriving from further depth [e.g., *Garcia et al.*, 2000]. Time series of variable isotope and trace element ratios suggest decadal-long periods of magma supply from a single shallow magma body, which alternates with those of two laterally distinct bodies [*Pietruszka et al.*, 2015]. Magma recharge from depth can be identified at Kīlauea by the eruption of high-MgO basalts or CO_2-rich olivine-hosted melt inclusions [e.g., *Anderson and Brown*, 1993].

Grímsvötn volcanic system, Iceland, being mostly subglacial is scarcely equipped with geophysical instruments, but nevertheless, a high-level magma chamber has been inferred from combined magnetic, gravity, seismic, and deformation studies [e.g., *Gudmundsson and Milsom*, 1997; *Alfaro et al.*, 2007; *Hreinsdóttir et al.*, 2014]. A low-velocity body with a volume of 10–20 km^3 was inferred at approximately 3–4 km depth by *Alfaro et al.* [2007], beneath which a dense mass of higher velocity is observed. Measured deformation before and during the 2011 eruption was interpreted by a Mogi model to give a point pressure source depth of 1.7 ± 0.2 km [*Hreinsdóttir et al.*, 2014], whereas the deformation pattern of Grímsvötn central volcano over a longer time period suggests at least two magma reservoirs [*Reverso et al.*, 2014]. Only basalt of relatively homogeneous and evolved tholeiitic composition is produced as tephra from the subglacial central

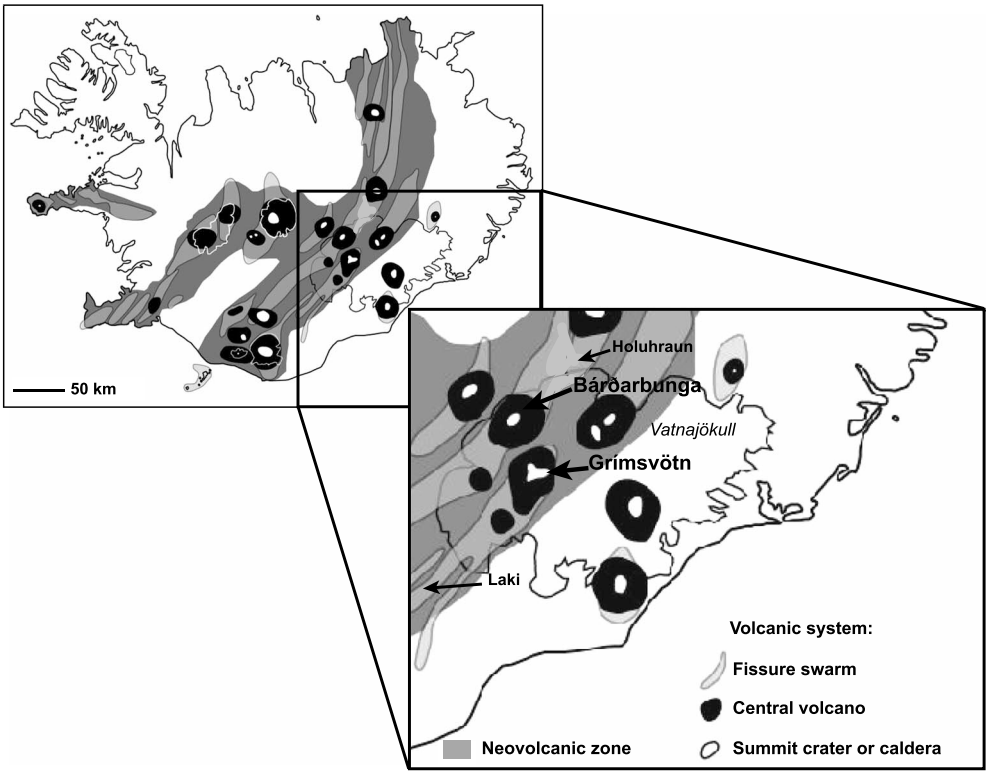

Figure 1. Map of South East Iceland showing Grímsvötn and Bárðarbunga volcanic systems partially located under the Vatnajökull ice cap. The volcanic systems are composed of a central volcano, hosting a caldera, and fissure swarms, at which occurred the basaltic fissure eruptions of Laki 1783–1784 and Holuhraun 2014–2015, respectively. Modified after *Jóhannesson and Sæmundsson* [1998].

volcano [*Óladóttir et al*., 2011a, 2011b] and lavas from the subaerial fissure swarm of similarly uniform composition, such as that of the Laki eruption [e.g., *Sigurdsson and Sparks*, 1978; *Sigmarsson et al*., 1991]. In order to better constrain the magma system beneath Grímsvötn, depth of crystallization at which magma resided is estimated through thermobarometry and phase equilibria. The results are compared with those obtained on the recent Holuhraun basalt, erupted in 2014–2015 on the adjacent Bárðarbunga volcanic system. Then, the petrological depth estimate of crystallization at these two volcanic systems is compared with results from large-scale magnetotelluric survey in southern Iceland [*Eysteinsson and Hermance*, 1985] and also with the inferred seismic layering of the Icelandic crust [e.g., *Bjarnason*, 2008]. In addition, sulfur and chlorine concentrations were measured in melt inclusions and groundmass glass from four historical eruptions, two larger events, and two smaller eruptions with an order of magnitude lower mass eruption rate. Their concentrations and degassing budget suggest a link between eruption regime, degassing efficiency, and volume of magma produced. The combined results permit evaluation of volatile-rich magma recharge in controlling different eruption regimes at Grímsvötn volcano.

2. Geological Setting

Grímsvötn and Bárðarbunga volcanic systems are located above the center of the Iceland mantle plume (Figure 1). For the former, most eruptions occur inside the subglacial Grímsvötn caldera, with a few notable exceptions such as the 1783–84 Laki and 1996 Gjálp events [e.g., *Thordarson and Self*, 1993; *Sigmarsson et al*., 2000]. Grímsvötn central volcano is the most active Icelandic volcano, erupting on average once per decade over the last eight centuries [*Larsen et al*., 1998]. The so-called Saksunarvatn ash, an important tephrochronological horizon from the very early Holocene, most likely originated at Grímsvötn [e.g., *Neave et al*., 2015]. Eruptions within the ice-covered part of the volcanic system are (i) predominantly phreatomagmatic in nature or (ii) alternating between phreatomagmatic activity and magmatic phases of subplinian/plinian intensity, termed here as plinian for simplification. Eruptions on the ice-free part are

predominantly effusive and able to produce flood basalts, such as the Laki lava fields. The order of magnitude smaller Holuhraun 2014–2015 eruption on the Bárðarbunga volcanic system produced more primitive basalt than Grímsvötn or olivine normative tholeiite [e.g., *Gudmundsson et al*., 2016]. Two of the four Grímsvötn eruptions studied here (1873 and 2011) are among the largest during the historical period (last thousand years approximately), whereas the remaining two (1823 and 2004) are typical of the more frequent low-intensity events (see further details in the supporting information [*Petersen et al*., 2012; *Thjódólfur*, 1873; *Thorarinsson*, 1974; *Thoroddsen*, 1924]).

3. Sample Description and Methods

3.1. Samples

The G1823 and G1873 tephra were collected in August 2005, approximately 25 km south of the Grímsvötn caldera, from tephra layers recently exposed in the ablation region of one of the outwash glaciers of Vatnajökull ice-cap (see sampling methods in *Larsen et al*. [1998]). Two decimetric bombs (G-2004-T2 and G-2004-T4) were selected from the 2004 eruption products collected from the crater inside the caldera wall. The near-vent lapilli-size tephra from the first eruption day in 2011 (sample G2011-D) and fine-grained tephra collected on the lowland, south of Vatnajökull (Gv4), represent the 2011 tephra. For comparison, results from a tephra produced early in the 2014–2015 Bárðarbunga rifting event were included in this study.

3.2. Melt Inclusion Preparation

Olivine, clinopyroxene, and plagioclase (hereafter abbreviated ol, cpx, and plag) crystals were handpicked under a binocular microscope from the 100–250 and 250–600 μm grain size fractions of crushed tephra. To facilitate the handpicking, dense liquids (bromoform and diiodomethane) were used to separate crystals from glass and plag from ferromagnesian minerals. Crystals with melt inclusions (MI) were washed with acetone, embedded in epoxy, and polished individually in order to generate adequate exposure of the MI for electron probe microanalysis (EPMA). The MI are spherical to oblate in shape and range in size from 5 to 190 μm in diameter. Most MI contain shrinkage bubbles but lack minerals and are primary melt inclusions [*Roedder*, 1984]. In total, 103 crystals containing 179 MI were selected and prepared for analysis. The groundmass of the 2011 tephra is composed of glass patches with variable microlite contents ranging from those that are completely free of microlites to heavily crystallized groundmass. From the G2011 tephra, a total of 49 cpx hosted 76 MI, and one olivine-hosted MI were obtained in addition to those of an earlier study [*Sigmarsson et al*., 2013] (Table S1 in the supporting information). From the G2004 tephra,12 cpx containing 33 MIs and six ol with seven MI were collected. In that of G1873, 10 cpx with 23 MI and two MI in two ol were analyzed and four cpx hosting nine MI from the G1823 tephra. *Sigmarsson et al*. [2013] showed that most MI in plag from the 2011 eruption had composition modified by host crystallization and O isotope ratios measured in plag from Grímsvötn products [*Bindeman et al*., 2006] are generally out of equilibrium with the groundmass glass. Therefore, plag was not studied in same details here as the ferromagnesian minerals. The groundmass glass around euhedral crystals was analyzed both adjacent to the crystal rims and elsewhere in each glass patch.

3.3. Microprobe Data Acquisition

Major and volatile (S, Cl, and F) element concentrations were measured on Cameca SX-100 at Laboratoire Magmas et Volcans in Clermont-Ferrand, France. A 15 keV accelerating voltage and a 15 nA current were used for the mineral analyses. The larger MI and groundmass glass were analyzed with a spot diameter of 20 μm and a current of 8 nA, whereas the smallest MI were analyzed with a 5 μm beam and a current as low as 4 nA. The secondary glass standard A99 was analyzed with a 5 μm beam. All results are given in Table S1. Reproducibility and accuracy were established by replicate analyses of VG-A99 glass standard for major element concentrations, Alvin glass standard for S concentrations, and Ke12 glass standard for Cl and F concentrations. Measured values of 0.100 ± 0.003 wt % for S in Alvin, 0.33 ± 0.01 wt % for Cl, and 0.46 ± 0.04 wt % for F in Ke12 are in good agreement with the published accepted values of these standards [*Óladóttir et al*., 2011a; *Moune et al*., 2007, and references therein]. For the concentration levels of Grímsvötn glass, the 1 SD ranges from 2 to 10% and 10 to 15%, respectively, on S and Cl concentrations. The detection limit for F concentration is between 200 and 300 ppm. The Kα ray position of sulfur was used to estimate fO_2 following *Carroll and Rutherford* [1988].

3.4. Test of Mineral-Melt Equilibrium and Geothermobarometry

Phase equilibrium is a prerequisite for application of thermobarometers based on mineral-liquid compositions and thermodynamic equilibrium. Three approaches are used here to assess the phase equilibrium, namely, textural criteria, calculated normalized mineral components, and equilibrium partition coefficients. Back-scattered electron (BSE) images revealed a few anhedral to subhedral crystals that were rejected from the *P-T* calculations. Most crystals selected for analysis are euhedral, suggesting textural equilibrium with their surrounding liquid (Table S1 and Figure S1 in the supporting information). In the case of zoned crystals, only rims and neighboring glass were used as representative of the last state of equilibrium between a given crystal and melt. The special case of sector-zoned cpx is discussed further below. The state of equilibrium was assessed from the ideal cpx end-member components (DiHd, EnFs, etc. [*Putirka*, 1999]; Figure S2). Final test of equilibrium was the criterion of Fe-Mg partitioning between ferromagnesian minerals and liquids: $K_D^{min-liq}$ (Fe-Mg) = $[MgO_{liq}*FeO_{min}]/[MgO_{min}*FeO_{liq}]$, where MgO and FeO are molar fractions. The equilibrium K_D value of 0.28 ± 0.08 between cpx and melt is used and 0.30 ± 0.03 for the ol-liquid equilibrium [e.g., *Roeder and Emslie*, 1970; *Herzberg and O'Hara*, 1998; *Toplis*, 2005; *Putirka*, 2008]. Clinopyroxene melt was used for *P-T* estimates because plag-liquid equilibrium constant $K_D^{fsp-liq}$(An-Ab) is not well constrained for tholeiitic magma, and the olivine crystals are rare.

Equilibrium crystallization temperatures (*T*) between ol, plag, cpx, and matrix glass were calculated respectively with equations 22, 24a, 33, and 13 of *Putirka* [2008, and references therein], with associated standard error of estimate (SEE) being 29, 36, 42, and 71°C, respectively. The crystallization pressure (*P*) estimates are based on clinopyroxene-liquid (cpx-liq) equilibrium using Putirka's equation 30 with a SEE of 1.6 kbar. The results are compared with *P* and *T* at which the phases olivine, plagioclase, augite, and melt are in equilibrium (OPAM; see the supporting information) [*Yang et al*., 1996]. The OPAM phase equilibria was already applied to estimate crystallization pressure for several Icelandic basalts [*Kelley and Barton*, 2008], whereas *Budd et al*. [2016] and *Geiger et al*. [2016] applied the *Putirka* [2008] cpx-liq barometer by selecting what they term as "appropriate nominal melt composition." In the absence of measurable liquid composition adjacent to the cpx due to highly palagonized glasses and/or crystallized groundmass in the studies of *Budd et al*. [2016] and *Geiger et al*. [2016], the authors suggest adoption of a "plausible whole-rock composition." However, *Óladóttir et al*. [2008, 2011b] demonstrated significant variability in glass composition of Holocene tephra from subglacial basalt volcanoes in Iceland. Thus, identifying a single "appropriate nominal melt composition" remains highly subjective and can lead to erroneous results. Comparing the empirically calculated cpx components to those analyzed is not a very stringent tool in evaluating equilibrium condition and only eliminates obscure analyses (such as occasional mixed glass-crystal rim analyses identified by monitoring K_2O concentrations). The problem with these approaches is perhaps best illustrated by the case of sector-zoned cpx (see further discussion in the supporting information [*Hammer et al*., 2016]). Two examples are given in Figure S3 illustrating that only analyses of euhedral mineral rims and the adjacent glass yield reasonable *P-T* results, whereas other cpx analyses yield erroneous results despite $K_D^{min-liq}$(Fe-Mg) (and cpx components) within accepted equilibrium range.

The approach preferred here was to calculate *P* and *T* only from analyses of crystal facets of the cpx phenocrysts in textural equilibrium with the adjacent glass, verified by BSE images, and the crystal cores enveloping glass inclusions. This ensures that only the relevant liquid and cpx compositions are utilized for the estimation of cpx crystallization pressure and temperature. Depth of cpx crystallization before two of the last three eruptions in Iceland, Eyjafjallajökull 2010 and Bárdarbunga 2014–2015, was estimated with this approach by *Keiding and Sigmarsson* [2012] and *Bali et al*. [2015]. In all three cases a strong agreement was found with depth estimates based on seismicity, minimum pressure derived from H_2O-CO_2 solubility, and GPS and interferometric synthetic aperture radar deformation data [e.g., *Tarasewicz et al*., 2012; *Gudmundsson et al*., 2016]. Recently, *Neave and Putirka* [2017] proposed a different calibration for calculating pressure of cpx crystallization with increased emphasis on results from 1 atm melting experiments. As discussed below, the application of their new calibration on two products from Grímsvötn volcanic system, the Laki basalt and the Saksunarvatn's tephra, yields results within error of those presented here on the four historical Grímsvötn tephra. However, their preferred calibration yields much lower *P* for experimental products at 5 and 10 kbar [*Haddadi*, 2016], whereas that of *Putirka* [2008] match the experimental results within error of that calibration. In addition, *P* estimates based on the OPAM phase equilibria are within error of the calibration of *Putirka*

[2008] that is therefore preferred in this paper. Nevertheless, it should be emphasized that only further experiments at *P* ranging from 1 atm to 5 kbar will permit refinement of the cpx-glass barometer.

3.5. Petrological Estimation of S Degassing

The petrological method for inferring S degassing is based on the difference (ΔS) between sulfur concentrations measured in phenocryst-hosted melt inclusions (MI), taken to indicate the preeruptive sulfur concentration dissolved in the parental melt, and the degassed groundmass glass representing the residual sulfur concentrations not emitted to the atmosphere [*Devine et al*., 1998]. Scaled to the mass of magma erupted ΔS yields the exsolved mass of sulfur, which can both form a gas phase (H_2S and SO_2) and precipitate as sulfide [*Sigmarsson et al*., 2013]. The petrological method estimates the mass of sulfur exsolved from the initial magma as follows: mass $SO_2 = \alpha\rho V_{DRE}$ ($S_{MI,max} - S_{Groundmass\ glass,\ mean}$), where α = MW (SO_2)/MW (S) = 64.06/32.06, ρ = 2750 kg m^{-3} for Grímsvötn magmas and the dense rock equivalent volume (V_{DRE}) from the eruption of interest.

4. Results

4.1. Petrography, Mineral, and Glass Compositions

The four Grímsvötn tephra are of quartz normative tholeiitic composition as are other Holocene Grímsvötn tephra [e.g., *Grönvold and Jóhannesson*, 1984; *Óladóttir et al*., 2011a, 2011b]. All four tephra have average MgO concentrations close to 5 wt %, in both the groundmass glass and the MI. Largest variability is observed for the 2011 tephra with a range from approximately 3 to 7 wt % with a bimodal distribution. Groundmass glass analyzed adjacent to euhedral crystals is of identical composition to that analyzed further away from the crystal rim. The tephra are composed of ~95% glass with only ~5% of visible crystals, namely, plag, cpx, and ol in decreasing abundances. Sulfide globules and FeTi-oxides were only observed in the G2011 tephra [*Sigmarsson et al*., 2013]. Representative mineral compositions are listed in Table S2. Plagioclase of the Grímsvötn 2011 tephra, which has the largest mineral compositional range of the four eruptions, varies from An_{55} to An_{76}, within the range found for the Saksunarvatn ash [*Neave et al*., 2015]. Still larger compositional range is observed in Laki products with macrocrysts ranging from An_{53} to An_{89} [*Neave et al*., 2013], extending the range (An_{75}-An_{90}) observed by *Bindeman et al*. [2006]. Macrocryst zonation is variable often with plag core, rich in Ca (An_{76}), frequently mantled by thick rim of lower Ca composition (An_{73}), whereas cpx occasionally shows complex sector zoning with a surrounding rim lower in Fe (Figure S3). These two principal mineral phases are both found as individual crystals but also forming glomerocrysts. Clinopyroxene is of augite composition with Mg # in the range of 73–84, within the range of those from the Saksunarvatn ash (Mg #: 71–87 [*Neave et al*., 2015]) and those of the Laki eruption (Mg #: 50–83 [*Neave et al*., 2013]). Olivines of the 2011 eruption have Fo values ranging from 68 to 77, which again is approximately within the range found in Saksunarvatn tephra (70–76 and 84–87 [*Neave et al*., 2015]). *Bindeman et al*. [2006] observed a Fo range of 72–86 in Laki macrocrysts, while *Neave et al*. [2013] measured Fo as low as 60. Larger variations are thus observed in mineral compositions of the larger Grímsvötn eruptions. Results on S and Cl concentrations and cpx crystallization pressure and temperature will first be presented for the two larger eruptions (in 2011 and 1873) and subsequently for the two smaller eruptions (those of 2004 and 1823).

Water and carbon dioxide concentrations were measured in a single melt inclusion by the ion probe (IMS 1270 instrument at Nancy, France). The results are 0.66 wt % H_2O and 960 ppm CO_2 (Table S2), which are comparable to 0.68 wt % H_2O measured in MI of olivines and plagioclases from the Saksunarvatn ash [*Neave et al*., 2015].

4.2. Sulfur and Chlorine

Sulfur and Cl are of concentration high enough to be measured by EMP, whereas the F concentrations are below the EMP detection limit (~300 ppm) and will not be further discussed. In the MI, the highest S and Cl concentrations, which range from 1103 to 1974 ppm and 112 to 339 ppm, respectively, are observed in MI of the larger eruptions (G1873 and G2011; Table 1 and Figure 2). Lower maxima S and Cl concentrations were obtained in MI of minerals of smaller eruptions (G1823 and G2004). Groundmass glass volatile concentrations vary significantly with S ranging from 407 to 1758 ppm and Cl from 142 to 307 ppm. Significantly, the weighted mean S concentrations of the combined groundmass glass of the larger two eruptions is significantly lower (~880 ppm) than that of the combined groundmass glass for the smaller eruptions

Table 1. Petrological Method Applied to Sulfur and Chlorine[a]

	Sulfur								Chlorine							
	G1823		G1873		G2004		G2011		G1823		G1873		G2004		G2011	
	ppm	±1σ	ppm	±1σ	ppm	±1σ	ppm	±1σ	ppm	±1σ	ppm	±1σ	ppm	±1σ	ppm	±1σ
Min(MI)	1386		1410		1220		1103		164		122		114		112	
Max(MI)	1731	65	1789	73	1667	75	1974	70	205	34	266	36	226	42	339	37
Mean(MI)	1571		1594		1443		1578		183		175		161		180	
Min(GG)	407		513		671		465		166		142		173		153	
Max(GG)	1758		1047		1586		1749		182		209		307		252	
Mean(GG)	1050	56	766	47	1138	62	908	55	210	13	180	27	227	39	208	34
ΔX	681	121	1023	120	539	137	1066	125	−5	47	86	63	−1	81	131	71
D_X (%)	39	8	57	9	32	10	54	8			32	28			39	25

[a]It is based on the difference between the maximum content in the melt inclusions minus the groundmass glass (GG) mean volatile concentration of the same element (i.e., X max MI – X mean GG = ΔX). Percentage of initial X available (D_X), which exsolved from the melt is $D_X = 100 * \Delta X/(X \text{ max MI})$. Multiplying ΔX by the dense rock equivalent volume of an eruption and by the mean density leads to the quantification of the mass emission of a given volatile (X). All analyses are given in Table S1

(~1100 ppm). Consequently, the difference between the maximum S concentrations in the MI minus mean S concentrations (ΔS) of the groundmass glass is significantly larger for the two larger eruptions (~1000 ppm) compared to ΔS of the smaller eruptions (~600 ppm). This observation is reinforced by higher ΔCl for the larger eruptions and negligible Cl degassing in tephra from the smaller two eruptions. Both chlorine and sulfur degassing thus appears hindered in the phreatomagmatic glass of the two smaller eruptions.

4.3. Pressure and Temperature of Partial Crystallization

4.3.1. Grímsvötn 2011

All the *P-T* calculations are performed assuming 0.6 wt % H_2O. Olivine-liquid temperature is estimated from a single MI-host-crystal pair giving 1212 ± 29°C, whereas the groundmass glass composition gives T in the range of 1100–1149°C. The cpx-liq thermometer for MI in cpx gives results between 1065 and 1175°C (Table 2), which display a near Gaussian distribution with a median centered on 1135°C (Figure 3). The lowest cpx-liquid temperature is close to the 1 atm experimental determined temperature for the appearance of FeTi-oxides on the liquidus, namely, 1070°C [*Bell and Humphries*, 1972], which were only observed in the G2011 tephra.

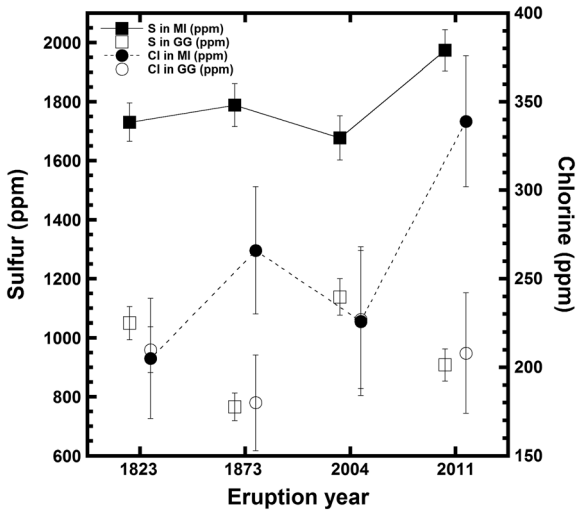

Figure 2. Concentrations of S (squares) and Cl (circles) in melt inclusions (filled symbols) and groundmass glass (open symbols) of four Grímsvötn eruptions. Chlorine did not form a volatile phase during the smaller 1823 and 2004 eruptions, resulting in identical concentrations in groundmass glass and clinopyroxene-hosted glass inclusions. See Table 1 for further information.

All MI pressure estimates from cpx-liquid equilibria are within the range of 0.6–6.4 kbar (mean 4.3 kbar). The frequency distribution in Figure 3 suggests that roughly 95% of the cpx crystallized between 2 and 6.4 kbar (MI mean: 4.3 kbar), while the rest originate from a shallower level corresponding to 0.6–1.5 kbar. Final *P-T* equilibrium of cpx crystallization is obtained from euhedral crystal rims and adjacent glass.

4.3.2. Grímsvötn 1873

Groundmass glass composition yields T range of 1125–1137°C, consistent with two olivine-liquid temperatures (1126 and 1129°C) for two MI in olivines having Fo_{73} and Fo_{74}, respectively. The MI in cpx formed at T between 1092 and 1150°C, with a mean of 1130°C (n = 21), which is indistinguishable (Table 2) to that obtained from the

Table 2. Result Summary of Temperature and Pressure Calculation for Four Historical Grímsvötn Eruptions[a]

		T Liq	T Ol-Liq	T Ol-MI	T Pl-MI	T Cpx-Liq	T Cpx-MI	P Cpx-Liq	P Cpx-MI
G1823	min	1126				1099	1108	−0.1	2.5
	max	1158				1163	1164	4.9	6.2
	median	1136				1141	1133	4.1	3.8
	mean	1139				1139	1133	3.5	3.9
	N	11				9	14	9	14
G1873	min	1125	1140	1126		1116	1092	2.6	2.0
	max	1137		1129		1157	1150	5.9	6.0
	median	1129		1128		1137	1129	3.9	4.0
	mean	1130		1128		1136	1130	4.0	4.1
	N	6	1	2		7	21	7	21
G2004	min	1073	1125			1082	1075	0.0	1.8
	max	1147				1148	1159	5.6	7.0
	median	1113				1129	1120	4.3	3.8
	mean	1116				1124	1120	3.7	3.8
	N	15	1			13	40	13	40
G2011	min	1100		1212	117	1082	1065	0.1	0.6
	max	1149			1165	1150	1175	4.5	6.4
	median	1128			1151	1116	1125	3.2	4.5
	mean	1129			1149	1118	1122	2.8	4.3
	N	21		1	21	10	82	10	82

[a]See Table S1 for the detailed results.

2011 tephra (given the associated error). Groundmass glass-cpx pairs *T* range is slightly wider (1075–1157°C) but their mean, 1129°C, is not different (n = 7).

The melt inclusions in cpx formed at *P* of 2.0–6.0 kbar with a mean *P* of 4.1 kbar (n = 21), again identical to what is observed for the products of the other large eruption (2011). Similar *P* is obtained for the final rim crystallization, or 2.6–5.9 kbar, with a mean of 4 kbar (n = 7).

4.3.3. Grímsvötn 2004 and 1823

Crystallization *T-P* conditions before the smaller eruptions are similar and thus discussed together. Olivine-hosted MIs were obtained for the 2004 eruption, with six crystals containing seven MI and two were surrounded by groundmass glass. Only a single pair has a K_D^{ol-liq}(Fe-Mg) within the equilibrium range, giving *T* of 1125 ± 29°C, identical to the mean groundmass glass-cpx *T* of 1124°C (range: 1082–1148°C; n = 13) for the 2004 eruption. For that of 1823, the cpx-liq *T* range from 1099 to 1163°C (mean 1139°C; n = 9). The groundmass glass-cpx barometry indicates crystallization from 0 to 5.6 kbar (mean 3.7 kbar, n = 13; Table 2 and Figure 3) and between −0.1 and 4.9 kbar (mean 3.5 kbar, n = 9) for the 2004 and 1823 products, respectively.

Similar *P-T* conditions are obtained for MI formations in cpx or *T* in the range of 1075–1159°C (mean 1120°C; n = 40) for the 2004 eruption, while fewer observations of the 1823 eruption product display a narrower range,1108–1164°C (mean 1133°C; n = 14), and *P* in the range 1.8 and 7.0 kbar (mean 3.8 kbar) and 2.5–6.2 kbar (mean 3.9 kbar) for the 2004 and 1823 eruptions, respectively.

4.3.4. Summary of Thermobarometric Results

The highest equilibrium pressure between cpx and MI exceeds 6 kbar for the four tephra studied. Crystallization at deeper depth cannot be excluded since only final equilibrium pressure is recorded in the crystal-melt composition during magma ascent. The average pressure of MI-cpx reaction for all four eruptions is 4.1 ± 1.1 (SD; Figure 4a and Table S1). This pressure compares well with OPAM phase equilibrium calculated from the Grímsvötn MI glass composition giving *P* = 4.8 kbar ±2.1 (SD) on average and 4.0 kbar ±1.7 (SD) from groundmass glass composition (Table S2).

The MI equilibrium temperature may suggest slow cooling of the Grímsvötn magma system with time. The youngest tephra (G2011 and G2004) record identical mean cpx-MI temperature, or 1120°C and 1122°C. Nominally higher temperature (1130°C) is calculated for the older G1873 and G1823 tephra, and highest preeruptive estimates of ~1140°C have been suggested for 1783–1784 Laki eruption and the ~10 ka Saksunarvatn tephra [*Bindeman et al.*, 2006; *Neave et al.*, 2015, and references therein]. Although these

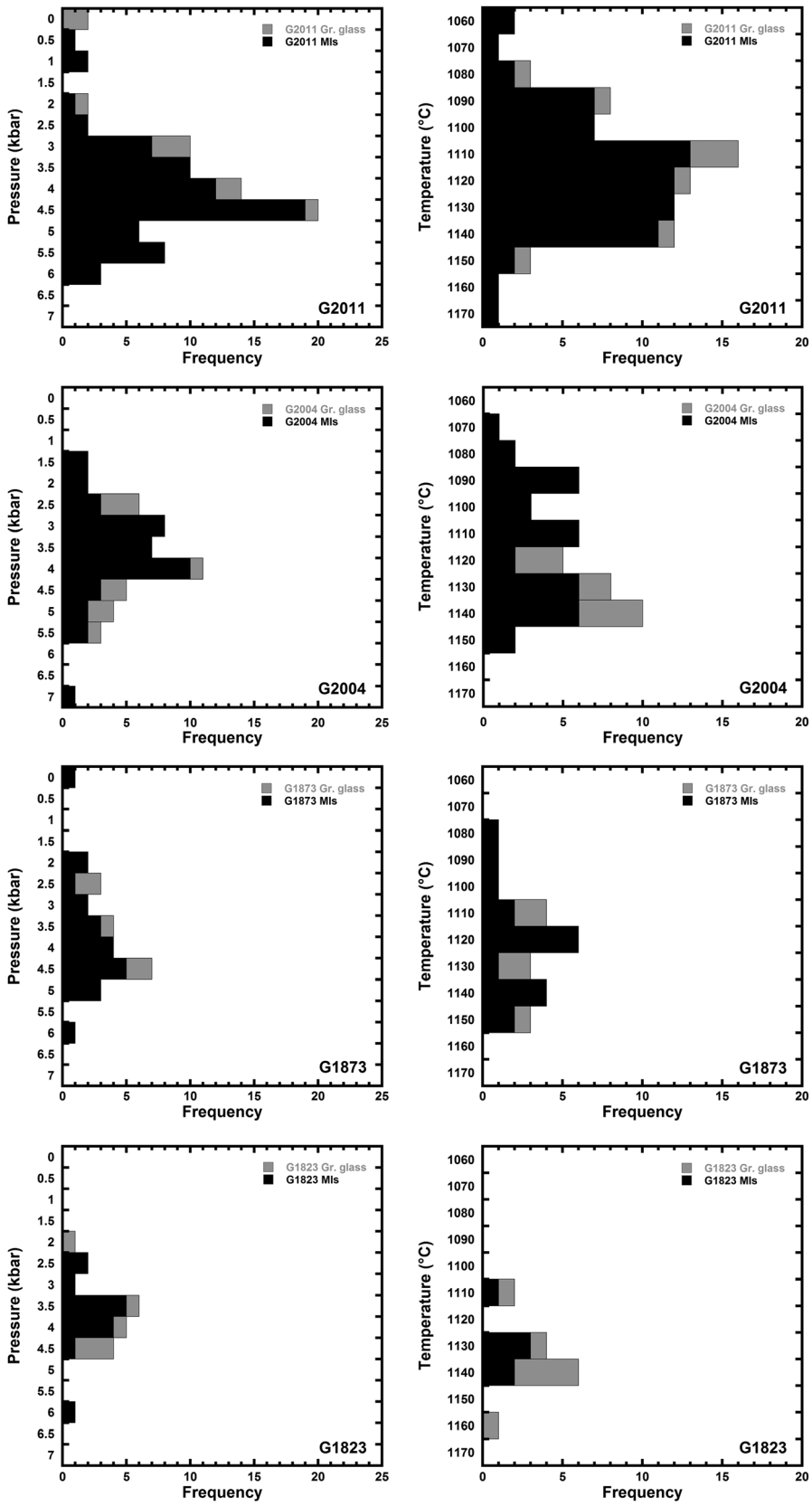

Figure 3. Grímsvötn thermobarometry results based on clinopyroxene and melt equilibrium in the four tephra samples studied. Melt inclusions and groundmass glass are abbreviated MI and Gr glass, respectively.

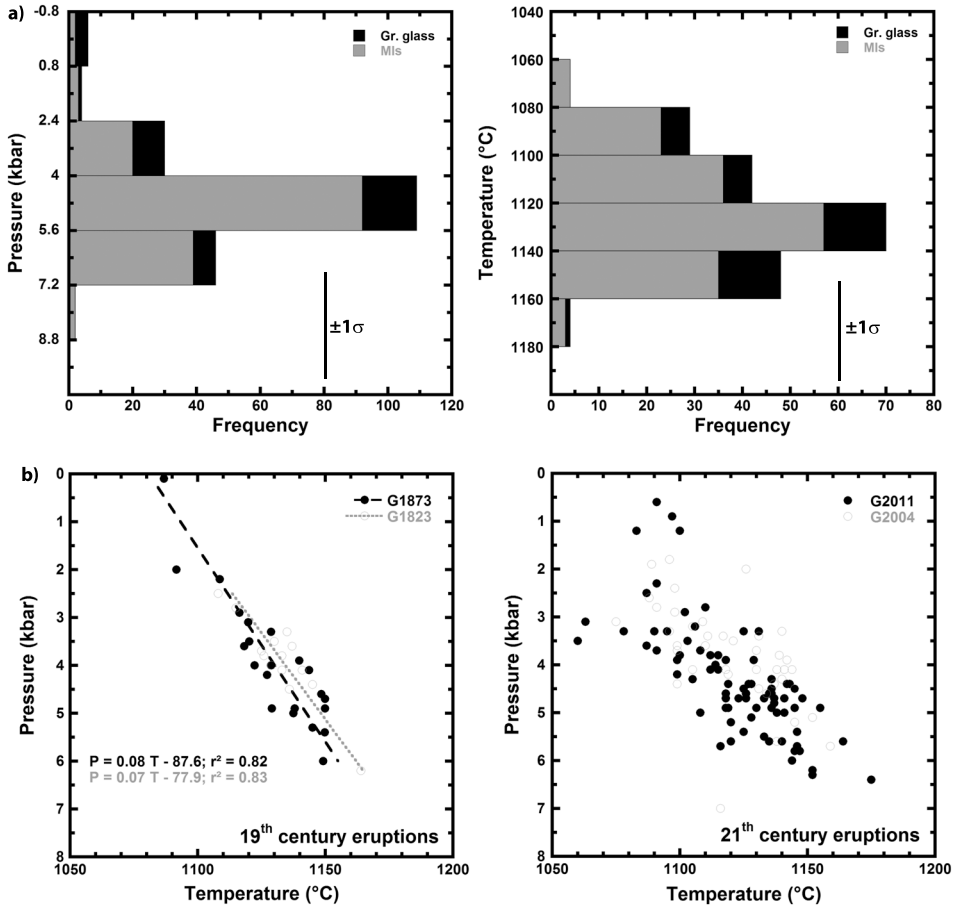

Figure 4. Pressure versus temperature from cpx-liq in Grímsvötn tephra. (a) Combined thermobarometry results from the four eruptions studied. (b) Linear correlation is observed only for the 19th century eruptions. The 21st century results suggest disconnected magma system at depth; see text for further discussion.

estimates are within the proposed thermometer errors [e.g., *Putirka*, 2008], similar pattern is observed in the final temperature recorded in cpx—groundmass glass thermometers (Table 2). A regular nominal decrease in calculated temperature with time is apparent (G1823 mean = 1139°C, G1873 mean = 1136°C, G2004 mean = 1124°C, and G2011 mean = 1118°C; Figure S4). Finally, the lowest recorded temperature, 1065°C, is from the G2011 tephra in which the presence of FeTi-oxides was identified for the first time in Grímsvötn products [*Sigmarsson et al.*, 2013].

5. Discussion

In this discussion both thermobarometry results and volatile concentrations measured in glasses of MI and groundmass are combined with the goal of putting constraints on the magma system behavior beneath Grímsvötn volcano.

5.1. Crystallization Depth and Magma Storage Beneath Grímsvötn

The average pressure recorded in the composition of the melt inclusions and clinopyroxene host crystals from the four Grímsvötn eruptions is approximately 4 kbar, whereas the spread in the results suggests crystallization within the entire crust, namely, cpx-hosted MI pressure between 0.6 and 7 kbar, i.e., 2 to 25 km. The results reveal the depth range of the magma system activated during each eruption and emphasize the frequency of cpx arising from approximately 15 km depth. Crystallization depth for two of the largest known or inferred eruptions at Grímsvötn, namely, the Laki and Saksunarvatn's eruptions, was studied by *Neave et al.* [2013, 2015], yielding a mean of 3.5–3.8 kbar (±1.0–0.6; 1 SD) for magnesian cpx and lower pressure for more

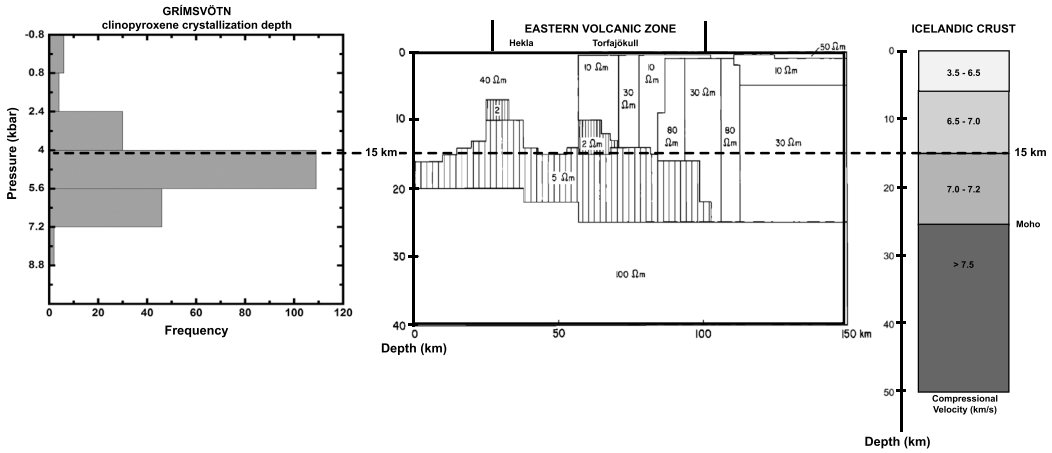

Figure 5. Clinopyroxene crystallization pressure estimated from equilibria with melt inclusions and groundmass glass from four Grímsvötn eruptions. The corresponding average depth estimate of 15 ± 5 km correlates with a layer of low-resistivity proposed by *Eysteinsson and Hermance* [1985] and the limit of middle-deep crust inferred from compressional seismic wave velocities [*Bjarnason*, 2008].

evolved cpx [*Neave and Putirka*, 2017]. Combined MI and groundmass glass compositions yield OPAM phase equilibria at P = 4.6 kbar ±2.0 (SD). These estimates thus give crystallization pressure within error of those obtained for the 1823, 1873, 2004, and 2011 eruptions at Grímsvötn. Consequently, it can be concluded that consistent results are obtained for the principal depth of Grímsvötn magma crystallization, namely, 13–17 km (3.5–4.8 kbar), and that different eruption magnitudes are not caused by difference in crystallization conditions.

In contrast to pressure, calculated equilibrium temperature appears to be time-dependent. Both ΔT of cpx-liq calculated from host crystal and MI and the ΔT calculated from the melt composition alone reveal a larger range for the 21st century eruption compared to that of the 19th century, or respectively 84–110°C and 56–58°C. This may suggest significant difference in thermal conditions between older and younger eruptions rather than between small and large eruptions at Grímsvötn. These differences could be explained by either different proportions and/or decreasing mixing efficiency of deep-derived basalts with more evolved high-level basalts today within the active magma system compared to the past. The lack of correlation between P and T for the 21st century eruptions may indeed suggest a magmatic system constituted of dykes and sills in which magma bodies are stored at different P and T conditions. The potential temperature decrease with time concurs with increasing concentrations of incompatible elements in historical Grímsvötn tephra caused by progressive fractional crystallization [*Sigmarsson et al*., 2016]. In Figure 4b the linear correlation between T and P for the 19th century eruptions is shown. Linear extrapolation of geothermal gradient in Iceland, as derived from geothermal exploration boreholes in Iceland, may indicate the depth to the 1200°C isotherm [*Flóvenz and Sæmundsson*, 1993]. Extrapolation of the cpx equilibrium crystallization P-T correlation yields a lower crustal pressure of 9 kbar for the 1200°C isotherm. Assuming an average crustal density of 2750 kg/m^3, a hydrostatic pressure of 9 kbar corresponds to approximately 30 km crustal depth. This depth corresponds to the estimated crustal thickness from seismic tomography [e.g., *Bjarnason*, 2008]. A crust-mantle boundary is likely to act as a neutral buoyancy level at which mantle melt can accumulate and from where the Grímsvötn magma system is supplied.

Ascending basaltic magma is stored higher up in the crust where cpx dominantly crystallizes. That depth corresponds to the limit of middle and lower crust as inferred from geophysical observations (Figure 5). The magnetotelluric survey of *Eysteinsson and Hermance* [1985] suggests a layer (~5 km thick) of low resistivity at similar depth across the Eastern Volcanic Zone of Iceland. This layer corresponds to the lower crust as proposed from compressional seismic velocity by *Bjarnason* [2008]. Similar crystallization depth is also observed from cpx-melt relationship in the 2014–2015 Holuhraun lavas (Table S3) despite their more primitive olivine tholeiite composition, which concurs with earlier results by *Bali et al*. [2015], *Gíslason et al*. [2015], and *Gudmundsson et al*. [2016]. An important magma crystallization and storage at approximately 15 ± 5 km depth is thus likely beneath the active volcanic systems of Iceland.

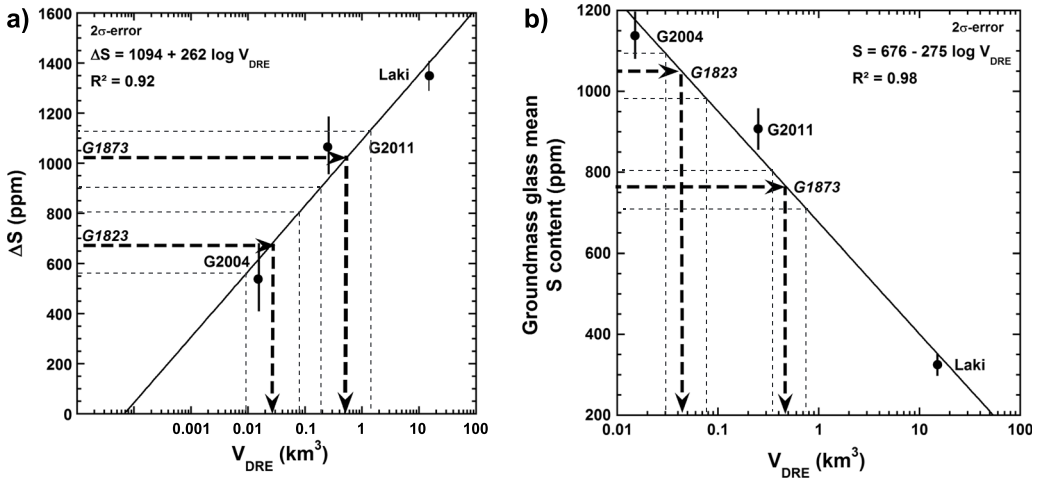

Figure 6. Relationship between the dense-rock-equivalent (DRE) volume and (a) the quantity of S exsolved (ΔS = S max MI − S mean groundmass glass; see text) and (b) the groundmass glass mean sulfur concentrations (in ppm) of different eruptions at the Grímsvötn volcanic system (volume estimates from *Thordarson and Self* [1993], *Jude-Eton et al.* [2012], and *Gudmundsson et al.* [2012]). The broken arrows highlight the V_{DRE} for the two 19th century eruptions estimated from the lognormal correlations.

5.2. Volatile Budget, Degassing, Eruption Volume, and Magma Recharge

Magma of the larger eruptions (1873 and 2011 tephra) erupted cpx-hosted MI with slightly higher S and Cl concentrations compared to those of the smaller phreatomagmatic eruptions (1823 and 2004 tephra; Figure 2). This suggests higher volatile concentrations in parental magma of the larger eruptions and/or higher proportions of magma recharge from depth compared to that of the smaller eruptions. Thus, the question whether different volatile concentrations contribute to the variable eruption regimes at Grímsvötn is worth exploring.

5.2.1. Sulfur and Eruption Volume

The maximum sulfur concentrations measured in the G2011 MI (max S = 1974 ppm; Table 1) and the average for the groundmass glass (908 ppm S) lead to 1.47 Tg of SO_2 exsolved from the initial magma using the petrologic method, which is within error of earlier estimate ([*Sigmarsson et al.*, 2013] ΔS values of 1066 versus 1063 ppm, respectively). For the Grímsvötn 2004 eruption, magma volume ($2.1 \pm 0.4 \times 10^{-2}$ km^3) estimated by *Jude-Eton et al.* [2012] gives 0.06 Tg of exsolved SO_2. How much of the sulfur was sequestered as sulfides and how much was emitted to the atmosphere cannot be evaluated due to lack of precise satellite observations during the small 2004 eruption. However, absence of sulfides in Grímsvötn tephra older than that of 2011 eruption suggests minimal S sequestration in sulfides of the older eruptions. The onset of titanomagnetite crystallization before the 2011 eruption corresponds to the progressive magma evolution at Grímsvötn during most of the historical period [*Sigmarsson et al.*, 2016]. Oxygen fugacity (fO_2), which is close to the FMQ-buffer, decreases with the titanomagnetite precipitation and that will stabilize sulfur as a sulfide species [e.g., *Jugo et al.*, 2010]. Relatively low fO_2 in the 2011 magma caused approximately 10% of the degassing sulfur as the reduced H_2S and important sulfur sequestration as sulfides [*Sigmarsson et al.*, 2013]. Absence of volume estimates for the 19th century tephra hampers discussion of exsolved SO_2, although crude estimations could be given using the determined ΔS (Figure 6a) for different eruptions on the Grímsvötn volcanic system.

For the Laki (1783–1784) eruption, *Thordarson et al.* [1996] estimated SO_2 emission of 122 Tg for a volume of 15.1 km^3, which corresponds to 8.1 Tg/km^3. The Grímsvötn 2011 eruption emitted 1.47 (±0.37) Tg for a volume of 0.25 (±0.05) km^3 which is equivalent to 5.9 Tg/km^3. *Hreinsdóttir et al.* [2014] estimated that 95% of the volcanic deformation occurred during the first 24 h corresponding to emission of 1.4 Tg SO_2 and a mean flux of 58 Gg of SO_2 per hour. In comparison, the Laki event may have produced 60% of its volatile emissions during the first 45 days [*Thordarson et al.*, 1996], which is equivalent to a mean flux of 68 Gg of SO_2 per hour. Hence, these two very different eruptions of the same volcanic system appear to have produced similar SO_2 fluxes. These fluxes are more than an order of magnitude higher than that observed

from the youngest flood basalt eruption in Iceland, namely, the Holuhraun 2014–2015 eruption (2.4 Gg/h on average [*Gauthier et al*., 2016]). The different SO_2 fluxes from Grímsvötn and Bárdarbunga eruptions are readily explained by higher volatile concentrations, and their incompatible element behavior, in the more evolved tholeiitic basalt produced at Grímsvötn.

There is an apparent relationship between dense rock equivalent (DRE) volume of erupted magma and its associated ΔS for eruptions at Grímsvötn volcanic system (Figure 6a). Magma volumes of the Laki, G2011, and G2004 eruptions correlate with ΔS, with a correlation coefficient (r^2) of 0.92. The Laki magma has the largest ΔS, that of 2011 an intermediate value and the phreatomagmatic 2004 eruption the lowest. Using the ΔS values measured (Table 1) for the 19th century eruptions, it is possible to evaluate their eruption volumes. Volume estimates of 3×10^{-2} km^3 for G1823 and 0.5 km^3 for G1873 are obtained, which are coherent with available written eruption descriptions (see Text S1 in supporting information). Although this relationship is only based on three observations, future Grímsvötn eruptions will serve to prove or reject this relationship.

Quantifying the S degassing, or rather the exsolution from the silicate liquid in case that part of the S is sequestered in sulfides, demonstrates the difference between the larger and the smaller eruptions. The relative exsolution is calculated as follows: $D_S = 100 * \Delta S/S_{initial}$, with $\Delta S = S_{initial} - S_{groundmass}$ ($S_{initial}$ = maximum S in MI), and leads to identical values for the plinian eruptions with D_S (G1873) ≈ D_S (G2011) ≈ 55% (Table 1). Significantly lower values are obtained for the phreatomagmatic events, or D_S (G1823) = 39% and D_S (G2004) = 32%. In part, this is caused by variable ΔS: ΔS (G2011) = 1066 ppm, close to ΔS (G1873) = 1023 ppm, whereas ΔS (G2004) = 539 ppm is close to ΔS (G1823) = 681 ppm. Therefore, the larger Grímsvötn eruptions not only had higher initial S concentrations but are also able to exsolve more sulfur than the smaller phreatomagmatic events. Obviously, the magma quenching effect due to efficient contact with glacial water arrests melt degassing of the less powerful eruptions. Higher mass eruption rate leads to lower water-melt contact and thus later melt quenching and enhanced outgassing. This is illustrated in Figure 6b, with increasing degree of degassing causing decreasing S concentrations in the groundmass glass in the order phreatomagmatic (1823 and 2004), plinian (1873 and 2011), and flood basalt eruptions (1783–1784 Laki). Similar phenomenon was observed for Holocene Katla tephra by *Óladóttir et al*. [2007]. If future eruptions from Grímsvötn confirm the proposed relationship between ΔS, groundmass S concentrations and magma volume erupted, then the volcano's production rate can be quantified from analysis of its historical tephra.

5.2.2. Chlorine

The degassing pattern of S is reflected by that of Cl. For G2011 and G1873 eruptions, the ΔCl is 131 ppm and 86 ppm, but the tephra of both phreatomagmatic eruptions have indistinguishable Cl concentrations in groundmass and MI glasses (Table 1 and Figure 2). Chlorine degassing could thus have been prevented by early quenching due to important water-melt interaction during the small eruptions, similar to the arrested S degassing. Alternatively, the fact that Cl solubility in basaltic melt is high [e.g., *Alletti et al*., 2009; *Lesne et al*., 2011], magma fragmentation may have occurred deeper than Cl volatilization. This latter possibility would imply, for a similar fragmentation depth, higher volatile content of the magma causing the larger eruptions.

The D_{Cl} (G2011) = 39% and D_{Cl} (G1873) = 32%, which leads to the mobilization of 0.1 Tg of HCl during the Grímsvötn 2011 eruption, using tholeiite magma density (2750 kg/m^3) and dense rock volume equivalent (0.27 km^3 [*Hreinsdóttir et al*., 2014]) of magma emitted. This atmospheric mass loading is thousand times higher than that (0.1 Mt HCl) of the Holuhraun 2014–2015 fissure eruption (1.6 km^3 [*Gíslason et al*., 2015]) despite an order of magnitude lower eruption volume. Chlorine concentrations are thus close to saturation in the quartz-normative tholeiitic melt under Grímsvötn. Taken together, the volatile results suggest degassing of sulfur before that of chlorine in the Grímsvötn tholeiites, as expected from the classical basaltic exsolution sequence of volatile elements, and higher volatile content in the magma of the larger eruptions.

5.2.3. Magma Recharge

Detailed tephrostratigraphy on the outlet glaciers of Vatnajökull (Figure 1) by *Larsen et al*. [1998] revealed a succession of high versus low eruption frequency phases at Grímsvötn volcano since at least the year 1200 Common Era (from the oldest tephra layer identified on the glaciers). A period of ~140 years and a similar duration of the two distinct phases, namely, 50–80 years, were identified. This conclusion is verified by the

138 years elapsing between the last two major Grímsvötn eruptions (2011 and 1873). These larger eruptions produce basalt with relatively high compatible element concentrations, such as Ni and Cr, attributed to magma recharge from depth [*Sigmarsson et al*., 2016]. Therefore, the larger explosivity of eruptions with plinian activity is most likely due to important recharge of deep-derived and volatile-rich magmas, supported by higher maximum sulfur and chlorine concentrations in melt inclusions of the plinian tephra (Figure 2). The initial volatile concentrations and the relative proportions of recharge magma versus residing magma thus appear to control the eruption regime at Grímsvötn volcano.

6. Conclusions

The principal conclusions are as follows:

1. Average pressure estimates of clinopyroxene crystallization in large and small eruptions at Grímsvötn volcano give of 4.1 ± 1.1 kbar, corresponding to approximately 15 ± 5 km depth. Absence of good temperature-pressure correlation for the 21st century eruptions suggests that the erupted magma derive from separated magma bodies with different thermal evolution, possibly in a plexus of sills and dikes.
2. Similar average crystallization depths of magma emitted in the four eruptions studied cannot explain different eruption regimes at Grímsvötn.
3. Sulfur and chlorine concentrations being highest in the melt inclusions of the larger eruptions (up to 1974 ppm and 339 ppm, respectively) are lowest in their groundmass glass. This indicates important recharge of deep-seated gas-rich magma at the origin of the tropopause-penetrating eruptions.
4. Quenching with glacial water explains higher volatile concentrations in groundmass glass for the smaller phreatomagmatic eruptions. The differences in volatile concentrations measured in melt inclusions and groundmass glass (i.e., ΔS) and the average concentration in the groundmass of each tephra appear to correlate with known eruptive volume for the 21st century eruptions and that of the Laki eruption, potentially permitting estimates of unknown volumes for older eruptions.

Acknowledgments
All analytical data pertinent to the conclusions of this paper are given in the supporting information. The Icelandic Glaciological Society, and especially Magnús T. Gudmundsson, made the sampling of the 19th century tephra possible. We are grateful to Jónas Guðnason who collected a proximal sample of the 2011 tephra; Andrés I. Guðmundsson, funded by the FP7 "FutureVolc" project, who assisted with mineral separations; and Jean-Luc Devidal for his expertise with the EPMA. Discussions with Bergrún Arna Óladóttir on Grímsvötn tephra, with Þorvaldur Þórðarson over the last three decades on the Laki eruption, and Didier Laporte on phase relationships are much appreciated. Constructive reviews by Mike Garcia and Mike Cassidy and the Editor, Luca Caricchi, considerably improved the manuscript. The PhD of the first author was financed by the Auvergne region in France. Field, travel, and analytical cost was covered by grants from the Iceland Research Fund project "Volcano Anatomy," the France-Iceland "Jules Verne" collaboration, and the French ANR project "DégazMag." This is a "ClerVolc" laboratory of excellence contribution 261.

References

Alfaro, R., B. Brandsdóttir, D. P. Rowlands, R. S. White, and M. T. Gudmundsson (2007), Structure of the Grímsvötn central volcano under the Vatnajökull icecap, Iceland, *Geophys. J. Int.*, *168*(2), 863–876, doi:10.1111/j.1365-246X.2006.03238.x.

Alletti, M., D. R. Baker, B. Scaillet, A. Auippa, R. Moretti, and L. Ottolini (2009), Chlorine partitioning between basaltic melt and H2O-CO2 fluids at Mount Etna, *Chem. Geol.*, *263*, 37–50.

Anderson, A. T., Jr., and G. G. Brown (1993), CO_2 contents and formation pressures of some Kilauean melt inclusions, *Am. Mineral.*, *78*, 794–803.

Bali, E., O. Sigmarsson, S. Jakobsson, and H. Gunnarsson (2015), Volatile-budget of the new fissure eruption of the Barðarbunga system, Iceland, *Geophys. Res. Abstr.*, *17*, EGU2015–5757.

Bell, J. D., and D. J. Humphries (1972), Lakagigar fissure eruption, in *Progress in Experimental Petrology*, *UK Publ. Ser.*, vol. D2, pp. 110–112, National Environmental Rec Council, London.

Bindeman, I., O. Sigmarsson, and J. Eiler (2006), Time constraints on the origin of large volume basalts derived from O-isotope and trace element mineral zoning and U-series disequilibria in the Laki and Grímsvötn volcanic system, *Earth Planet. Sci. Lett.*, *245*(1–2), 245–259, doi:10.1016/j.epsl.2006.02.029.

Bjarnason, I. T. (2008), An Iceland hotspot saga, *Jökull*, *58*, 3–16.

Budd, D. A., V. R. Troll, B. Dahren, and S. Burchardt (2016), Persistent multitiered magma plumbing system beneath Katla volcano, Iceland, *Geochim. Geophys. Geosyst.*, *17*, 966–980, doi:10.1002/2015GC006118.

Carroll, M. R., and M. J. Rutherford (1988), Sulfur speciation in hydrous experimental glasses of varying oxidation states: Results from measured wavelength shifts of sulfur X-ray, *Am. Mineral.*, *73*, 845–849.

Devine, J. D., H. Sigurdsson, A. N. Davis, and S. Self (1998), Estimates of sulfur and chlorine yield to the atmosphere from volcanic eruptions and potential climatic effects, *J. Geophys. Res.*, *89*, 6309–6325, doi:10.1029/JB089iB07p06309.

Eysteinsson, H., and J. F. Hermance (1985), Magnetotelluric measurements across the eastern neovolcanic zone in south Iceland, *J. Geophys. Res.*, *90*, 10,093–10,103, doi:10.1029/JB090iB12p10093.

Flóvenz, Ó. G., and K. Sæmundsson (1993), Heat flow and geothermal processes in Iceland, *Tectonophysics*, *225*, 123–138.

Garcia, M. O., A. J. Pietruszka, J. M. Rhodes, and K. Swanson (2000), Magmatic processes during the prolonged Pu'u 'O'o eruption of Kilauea volcano, Hawaii, *J. Petrol.*, *41*, 967–990, doi:10.1093/petrology/41.7.967.

Gauthier, P.-J., O. Sigmarsson, M. Gouhier, B. Haddadi, and S. Moune (2016), Elevated gas flux and trace metal degassing from the 2014–2015 fissure eruption at the Bárðarbunga volcanic system, Iceland, *J. Geophys. Res. Solid Earth*, *121*, 1610–1630, doi:10.1002/2015JB012111.

Geiger, H., T. Mattson, F. M. Deegan, V. R. Troll, S. Burchardt, Ó. Gudmundsson, A. Tryggvason, M. Krumbholz, and C. Harris (2016), Magma plumbing for the 2014–15 Holuhraun eruption, Iceland, *Geochim. Geophys. Geosyst.*, *17*, 966–980, doi:10.1002/2016GC006317.

Gíslason, S. R., et al. (2015), Environmental pressure from the 2014–15 eruption of Bárðarbunga volcano, Iceland, *Geochem. Perspect. Lett.*, *1*, 84–93, doi:10.7185/geochemlet.1509.

Grönvold, K., and H. Jóhannesson (1984), Eruption in Grímsvötn 1983, *Jökull*, *34*, 1–11.

Gudmundsson, M. T., and J. Milsom (1997), Gravity and magnetic studies of the subglacial Grímsvötn volcano, Iceland: Implications for crustal and thermal structure, *J. Geophys. Res.*, *102*, 7691–7704, doi:10.1029/96JB03808.

Gudmundsson, M.T., et al. (2012), The May 2011 eruption of Grímsvötn, *Geophys. Res. Abstr.*, *14*, EGU2012-12119.

Gudmundsson, M. T., et al. (2016), Gradual caldera collapse at Bárðarbunga volcano, Iceland, regulated by lateral magma outflow, *Science*, *353*, doi:10.1126/science.aaf8988.

Haddadi, B. (2016), Ascension et dégazage des magmas basaltiques: Application aux volcans d'Islande et de la Chaîne des Puys (France), PhD thesis, 307 pp., Université Blaise Pascal - Clermont-Ferrand II.
Hammer, J., S. Jacob, B. Welsch, E. Hellebrand, and J. Sinton (2016), Clinopyroxene in postshield Haleakala ankaramite: 1. Efficacy of thermobarometry, *Contrib. Mineral. Petrol.*, *171*(1), 7.
Herzberg, C., and M. J. O'Hara (1998), Phase equilibrium constraints on the origin of basalts, picrites, and komatiites, *Earth Sci. Rev.*, *44*, 39–79.
Hreinsdóttir, S., et al. (2014), Volcanic plume height correlated with magma-pressure change at Grímsvötn Volcano, Iceland, *Nat. Geosci.*, *7*(3), 214–218, doi:10.1038/ngeo2044.
Jóhannesson, H., and K. Saemundsson (1998), Geological map of Iceland: 1:500 000 bedrock geology, Icelandic Institute of Natural History, Reykjavik.
Jude-Eton, T. C., T. Thordarson, M. T. Gudmundsson, and B. Oddsson (2012), Dynamics, stratigraphy and proximal dispersal of supraglacial tephra during the ice-confined 2004 eruption at Grímsvötn Volcano, Iceland, *Bull. Volcanol.*, *74*(5), 1057–1082, doi:10.1007/s00445-012-0583-3.
Jugo, P. J., M. Wilke, and R. E. Botcharnikov (2010), Sulfur K-edge XANES analysis of natural and synthetic basaltic glasses: Implications for S speciation and S content as function of oxygen fugacity, *Geochim. Cosmochim. Acta*, *74*(20), 5926–5938, doi:10.1016/j.gca.2010.07.022.
Keiding, J. K., and O. Sigmarsson (2012), Geothermobarometry of the 2010 Eyjafjallajökull eruption: New constraints on Icelandic magma plumbing systems, *J. Geophys. Res.*, *117*, B00C09, doi:10.1029/2011JB008829.
Kelley, D. F., and M. Barton (2008), Pressures of crystallization of Icelandic magmas, *J. Petrol.*, *49*(3), 465–492, doi:10.1093/petrology/egm089.
Larsen, G., M. T. Gudmundsson, and H. Björnsson (1998), Eight centuries of periodic volcanism at the center of the Iceland hotspot revealed by glacier tephrostratigraphy, *Geology*, *26*, 943–946.
Lesne, P., S. C. Kohn, J. Blundy, F. Witham, R. E. Botcharnikov, and H. Behrnes (2011), Experimental simulation of closed-system degassing in the system basalt-H_2O-CO2-S-Cl, *J. Petrol.*, *52*, 1737–1762, doi:10.1093/petrology/egr027.
Moune, S., O. Sigmarsson, T. Thordarson, and P. J. Gauthier (2007), Recent volatile evolution in the magmatic system of Hekla volcano, Iceland, *Earth Planet. Sci. Lett.*, *255*(3–4), 373–389, doi:10.1016/j.epsl.2006.12.024.
Neave, D. A., and K. D. Putirka (2017), A new clinopyroxene-liquid barometer, and implications for magma storage pressures under Icelandic rift zones, *Am. Mineral.*, *102*, 777–794.
Neave, D. A., E. Passmore, J. Maclennan, G. Fitton, and T. Thordarson (2013), Crystal-melt relationships and the record of deep mixing and crystallization in the AD 1783 Laki eruption, Iceland, *J. Petrol.*, *54*(8), 1661–1690, doi:10.1093/petrology/egt027.
Neave, D. A., J. Maclennan, T. Thordarson, and M. E. Hartley (2015), The evolution and storage of primitive melts in the Eastern Volcanic Zone of Iceland: The 10 ka Grímsvötn tephra series (i.e. the Saksunarvatn ash), *Contrib. Mineral. Petrol.*, *170*(2), 21, doi:10.1007/s00410-015-1170-3.
Óladóttir, B. A., T. Thordarson, G. Larsen, and O. Sigmarsson (2007), Survival of the Mýrdalsjökull ice-cap through the Holocene thermal maximum: Evidence from sulfur contents in Katla tephra layers (Iceland) from the last ~8400 years, *Ann. Glaciol.*, *45*, 183–188.
Óladóttir, B. A., O. Sigmarsson, G. Larsen, and T. Thordarson (2008), Katla volcano, Iceland: Magma composition, dynamics and eruption frequency as recorded by Holocene tephra layers, *Bull. Volcanol.*, *70*, 475–493, doi:10.1007/s00445-007-0150-5.
Óladóttir, B. A., G. Larsen, and O. Sigmarsson (2011a), Holocene volcanic activity at Grímsvötn, Bárðarbunga and Kverkfjöll subglacial centres beneath Vatnajökull, Iceland, *Bull. Volcanol.*, *73*(9), 1187–1208, doi:10.1007/s00445-011-0461-4.
Óladóttir, B. A., O. Sigmarsson, G. Larsen, and J.-L. Devidal (2011b), Provenance of basaltic tephra from Vatnajökull subglacial volcanoes, Iceland, as determined by major- and trace-element analyses, *The Holocene*, *21*(7), 1037–1048, doi:10.1177/0959683611400456.
Petersen, G. N., H. Bjornsson, P. Arason, and S. von Löwis (2012), Two weather radar time series of the altitude of the volcanic plume during the May 2011 eruption of Grímsvötn, Iceland, *Earth Syst. Sci. Data*, *4*, 121–127, doi:10.5194/essdd-5-281-2012.
Pietruszka, A. J., D. E. Heaton, J. P. Marske, and M. O. Garcia (2015), Two magma bodies beneath the summit of Kilauea Volcano unveiled by isotopically distinct melt deliveries from the mantle, *Earth Planet. Sci. Lett.*, *413*, 90–100, doi:10.1016/j.epsl.2014.12.040.
Poland, M. P., A. Miklius, and E. K. Montgomery (2014), Magma supply, storage, and transport at shield-stage Hawaiian volcanoes, in *Characteristics of Hawaiian Volcanoes*, edited by M. P. Poland, T. J. Takahashi, and C. M. Landowski, chap. 5, *U.S. Geol. Surv. Prof. Pap.*, 1801, 179–234, Washington.
Putirka, K. D. (1999), Clinopyroxene + liquid equilibria to 100 kbar and 2450 K, *Contrib. Mineral. Petrol.*, *135*, 151–163.
Putirka, K. D. (2008), Thermometers and barometers for volcanic systems, *Rev. Mineral. Geochem.*, *69*(1), 61–120, doi:10.2138/rmg.2008.69.3.
Reverso, T., J. Vandemeulebrouck, F. Jouanne, V. Pinel, T. Villemin, E. Sturkell, and P. Bascou (2014), A two-magma chamber model as a source of deformation at Grímsvötn Volcano, Iceland, *J. Geophys. Res. Solid Earth*, *119*, 4666–4683, doi:10.1002/2013JB010569.
Roedder, E. (1984), Fluid inclusions, in *Reviews in Mineralogy*, vol. 12, p. 644, Mineral. Soc. Am., Chantilly.
Roeder, P. L., and R. F. Emslie (1970), Olivine-liquid equilibrium, *Contrib. Mineral. Petrol.*, *29*, 275–289, doi:10.1007/BF00371276.
Sigmarsson, O., M. Condomines, K. Grönvold, and T. Thordarson (1991), Extreme magma homogeneity in the 1783–84 Lakagigar eruption: Origin of large volume of evolved basalt in Iceland, *Geophys. Res. Lett.*, *18*, 2229–2232, doi:10.1029/91GL02328.
Sigmarsson, O., H. Karlsson, and G. Larsen (2000), The 1996 and 1998 subglacial eruptions beneath Vatnajökull glacier in Iceland: Contrasting geochemical and geophysical inferences on magma migration, *Bull. Volcanol.*, *61*, 468–476.
Sigmarsson, O., B. Haddadi, S. Carn, S. Moune, J. Gudnason, K. Yang, and L. Clarisse (2013), The sulfur budget of the 2011 Grímsvötn eruption, Iceland, *Geophys. Res. Lett.*, *40*, 6095–6100, doi:10.1002/2013GL057760.
Sigmarsson, O., M. Carpentier, G. Larsen, and M. T. Gudmundsson (2016), Magma fluxes and storage beneath Grímsvötn volcano, Iceland, estimated from ice-kept historical tephra, *Geophys. Res. Abstr.*, *18*, EGU2016–10185.
Sigurdsson, H., and R. S. J. Sparks (1978), Lateral magma flow within rifted Icelandic crust, *Nature*, *274*, 126–130.
Tarasewicz, J., R. S. White, A. W. Woods, B. Brandsdóttir, and M. T. Gudmundsson (2012), Magma mobilization by downward-propagating decompression of the Eyjafjallajökull volcanic plumbing system, *Geophys. Res. Lett.*, *39*, L19309, doi:10.1029/2012GL053518.
Thjódólfur (1873), 25, February 26th, pp. 61-62.
Thorarinsson, S. (1974), *Vötnin stríð. Saga Skeiðarárhlaupa og Grímsvatnagosa (the Swift Flowing Rivers. Annals of jökulhlaups in the River Skeidará and Eruptions of Grímsvötn)*, p. 254, Bókaútgáfa Menningarsjóðs, Reykjavik, Iceland.
Thordarson, T., and S. Self (1993), The Laki (Skaftár Fires) and Grímsvötn eruptions in 1783–1785, *Bull. Volcanol.*, *55*(4), 233–263.
Thordarson, T., S. Self, N. Oskarsson, and T. Hulsebosch (1996), Sulfur, chlorine, and fluorine degassing and atmospheric loading by the 1783–1784 AD Laki (Skaftár Fires) eruption in Iceland, *Bull. Volcanol.*, *58*, 205–225, doi:10.1007/s004450050136.
Thoroddsen, Th. (1924), Fjórar ritgjördir, Safn Frædafélagsins um Island og Islendinga, Copenhagen.
Toplis, M. J. (2005), The thermodynamics of iron and magnesium partitioning between olivine and liquid: Criteria for assessing and predicting equilibrium in natural and experimental systems, *Contrib. Mineral. Petrol.*, *149*(1), 22–39, doi:10.1007/s00410-004-0629-4.
Yang, H.-J., R. J. Kinzler, and T. L. Grove (1996), Experiments and models of anhydrous, basaltic olivine-plagioclase-augite saturated melts from 0.001 to 10 kbar, *Contrib. Mineral. Petrol.*, *124*, 1–18, doi:10.1007/s0041000501.